The Nuclear–Cytoskeletal Interface Is a Vulnerability in Aging Endothelium

Caitlin Francis[1,2], Felipe Leser[1,2], Roberto Lopez[1,2], Anne Eichmann[1-3*]

1 Cardiovascular Research Center, Department of Internal Medicine, Yale University School of Medicine, New Haven, CT, USA

2 Department of Molecular, Cellular and Developmental Biology, Yale University School of Medicine, New Haven, CT, USA

3 Paris Cardiovascular Research Center, Inserm U970, Université Paris, Paris, France

* Corresponding author, email: anne.eichmann@yale.edu

Abstract

Vascular aging is a fundamental driver of age-related cardiovascular diseases. Endothelial cells (ECs) lining the vascular lumen of capillaries are specialized, thin cells that supply tissues with metabolites, and their loss in aging poses a threat to tissue perfusion and ischemia risk. Mechanisms causing capillary dropout in aging are largely unknown, although VEGF signaling deficiency is implicated.[15] To identify mechanisms involved in vascular aging, we investigated mice with the accelerated aging disorder Progeria, and aged wildtype mice. At the organismal level, Progerin expression reduced sprouting angiogenesis and capillary density in neonatal mouse retinas, which impaired tissue perfusion and increased DNA damage compared to wildtype littermates. Progeric capillaries and aortic ECs displayed a disrupted nuclear-cytoskeletal interface that was shared with aged wildtype mice. 4D EC sprouts derived from Progeria mice had mispositioned nuclei at sprouting tips and bulging nuclei that failed to flatten and obstructed lumen formation, demonstrating cell autonomous defects. Progerin expression in human ECs likewise affected nuclear positioning and flattening and prevented sprouting and lumen formation. Mechanistically, Progerin expression altered LINC complex protein abundance resulting in a failed connection with cytoskeletal Actin and the intermediate filament protein Vimentin. Impairment of the nuclear-cytoskeletal interface was conserved in Progeria patient derived ECs, and partially rescued by inhibiting Progerin with the drug, Progerinin. Taken together, our results reveal that nuclear positioning and flattening is required for angiogenic sprouting and lumen formation respectively and identify the nuclear-cytoskeletal interface as a vulnerability for age-related microvascular dropout and a target for therapeutic intervention.

Introduction

Vascular aging is the gradual deterioration of the structure and function of blood vessels over a lifetime and is considered as the fundamental underlying driver of many age-related cardiovascular diseases (CVDs). As the primary risk factor for CVD, which remains the leading cause of morbidity and mortality worldwide, studying vascular aging is crucial for improving health span, fostering healthy aging, and reducing the rising global economic and social burden of disease.[1]

Cardiovascular functional decline varies among individuals of the same chronological age, prompting the search for biomarkers of functional aging to identify individuals at risk and identify the genetic, molecular, and cellular mechanisms underlying CVD initiation, progression, and complications.[24] Hutchinson-Gilford Progeria Syndrome (hereafter Progeria) is a premature aging syndrome that results in CVD and death from complications of atherosclerosis such as myocardial infarction, heart failure, or stroke at a mean age of 14.5 years.[16, 17] Research into Progeria helped identify mechanisms underlying CVD independently of risk factors or aging-associated chronic diseases that can influence cardiovascular health. Notably, Progerin is expressed at low level in aged tissues of non-HGPS individuals, suggesting a role in normal aging.[16] Understanding how Progerin causes CVD and an accelerated aging phenotype may therefore shed some light on normal aging.

Children with Progeria acquire a de novo germline heterozygous mutation within exon 11 of Lamin-A, which results in aberrant expression of a splicing isoform termed Progerin.[12] Normal Lamin-A encodes an essential nuclear scaffolding protein that lines the inner nuclear membrane and helps regulate nuclear shape, size, and mechanics. The Progerin isoform causes nuclear deformation and abnormal nuclear morphology, leading to a broad spectrum of heterochromatin loss, mis-localization and loss of DNA damage repair proteins and chromatin-associated proteins, along with mitochondrial and telomere dysfunction.[2,3] This results in accelerated cell senescence and loss of vascular smooth muscle cells (VSMCs), paralleled by reduced contractility, excessive deposition of extracellular matrix, and medial calcification.[32] VSMC loss and resulting atherosclerotic disease have been extensively studied in Progeria, but the effects of Progerin on the endothelial cells at the inner lining of blood vessels are less well understood.

In the microvasculature, nutrient exchanges with tissues depend on the 200 nm thin layer of endothelium, with the endothelial nuclei also flattening to accommodate blood flow.[26] Nuclear position and shape are central to endothelial sprouting angiogenesis, lumen hollowing, and lumen maintenance, but how these processes are regulated remains poorly understood. Nuclear mechanics are governed by the Linker of Nucleoskeleton and Cytoskeleton (LINC) complex composed of Nesprin, Sun and Lamin proteins which work in concert to anchor microtubules, intermediate filaments and actin to the nuclear membrane.[4,10,22] Evidently, the nuclear lamina integrity is paramount to a healthy vascular system, but how Progeria affects the endothelial cells in large and small vessels remains to be uncovered. Nuclear flattening is a coordinated effort which requires the LINC complex to achieve whilst not altering or damaging chromatin.[11] In general, little is known about how the endothelial nucleus achieves movement and shape changes during vessel sprouting and even less is known regarding how a disrupted

nuclear lamina, caused by Progerin expression, would impact these phenomena. Our work sought to identify both the molecular mechanisms of endothelial nuclear movement as well as how Progerin expression effects these mechanisms.

Previous work by Chancellor and colleagues report actomyosin tension exerted on the nucleus through Nesprin1 influences endothelial cell adhesion, migration and reorientation.[6] Similarly, multiple reports exist suggesting Nesprins of the LINC complex is required for endothelial cell adhesion, migration, and adaptation to shear stress and cyclic stretch.[10, 22] These reports indicate that LINC complex proteins are critical to endothelial function, yet the contribution of Lamin-A is unclear. Moreover, the extent to which Lamin-A mutation drives a vascular aging phenotype remains elusive.

We demonstrate that the microvasculature of human-Progerin–expressing mice exhibits delayed vascular development, lumen collapse, increased DNA damage, abnormal cytoskeletal protein localization, and reduced tissue perfusion. Ex vivo sprouting assays using isolated endothelial cells from mutant mice indicate that these defects arise in an endothelial cell autonomous manner. Furthermore, using patient-derived induced pluripotent stem cells differentiated into endothelial cells and cultured in 3D sprouting assays, we observed aberrant nuclear positioning, cytokinetic defects, and a failure of nuclei to undergo shape changes during lumen hollowing. Through extensive biochemical analyses, we linked these abnormalities to a reduced mechanical interface between the nucleus and the cytoskeletal proteins actin and vimentin.

Notably, the loss of perinuclear vimentin observed in Progeric mice was also evident in aged mice, revealing a shared cytoskeletal defect between Progeria and normal aging. This finding provides a potential mechanistic bridge between these conditions, which have long been linked phenotypically but lack clear molecular convergence. Supporting this idea, a case study by Cogné and colleagues reported that a mutation in vimentin produces a premature aging phenotype, implicating vimentin dysfunction in age-related pathology.[9] Together, these observations suggest that disruption of vimentin-mediated nucleo–cytoskeletal coupling may represent a conserved mechanism contributing to vascular decline in both Progeria and physiological aging. Importantly, treatment with Progerinin, a chemically modified Lamin A inhibitor, partially restored nucleo–cytoskeletal connectivity, highlighting the therapeutic potential of targeting this pathway.

Together, our results support a model in which endothelial nuclear mobility depends on coordinated interactions between the LINC complex and the actin and vimentin cytoskeletal networks. Progerin expression alters the abundance of SUN and Nesprin proteins at the nuclear envelope, weakening connections to actin and vimentin, which leads to global cytoskeletal dysfunction and subsequent microvascular defects.

Results

Progerin Expression in Mice Delays Retinal Angiogenesis

We analyzed mice expressing human Progerin (LMNA G608G), which recapitulate hallmarks of the human disease and exhibit a reduced lifespan of <25 weeks in our facility. The body weight

of homozygous Progeric pups was already significantly lower than wildtype controls at postnatal day (P)6, while hemizygotes showed an intermediate phenotype (**Figure 1a**) and remained reduced throughout the lifespan (**Supplemental Figure 1a-c**). We assessed whether Progerin expression impacted vascular development in the retina, which occurs along a well-defined postnatal timeline that can be quantified in the whole organ using isolectin-B4 (IB4) staining of endothelial cells. At P6, retinal outgrowth and vessel density were significantly delayed in homozygous Progeric mice compared to hemizygous and controls (**Figure 1b-d**). At the

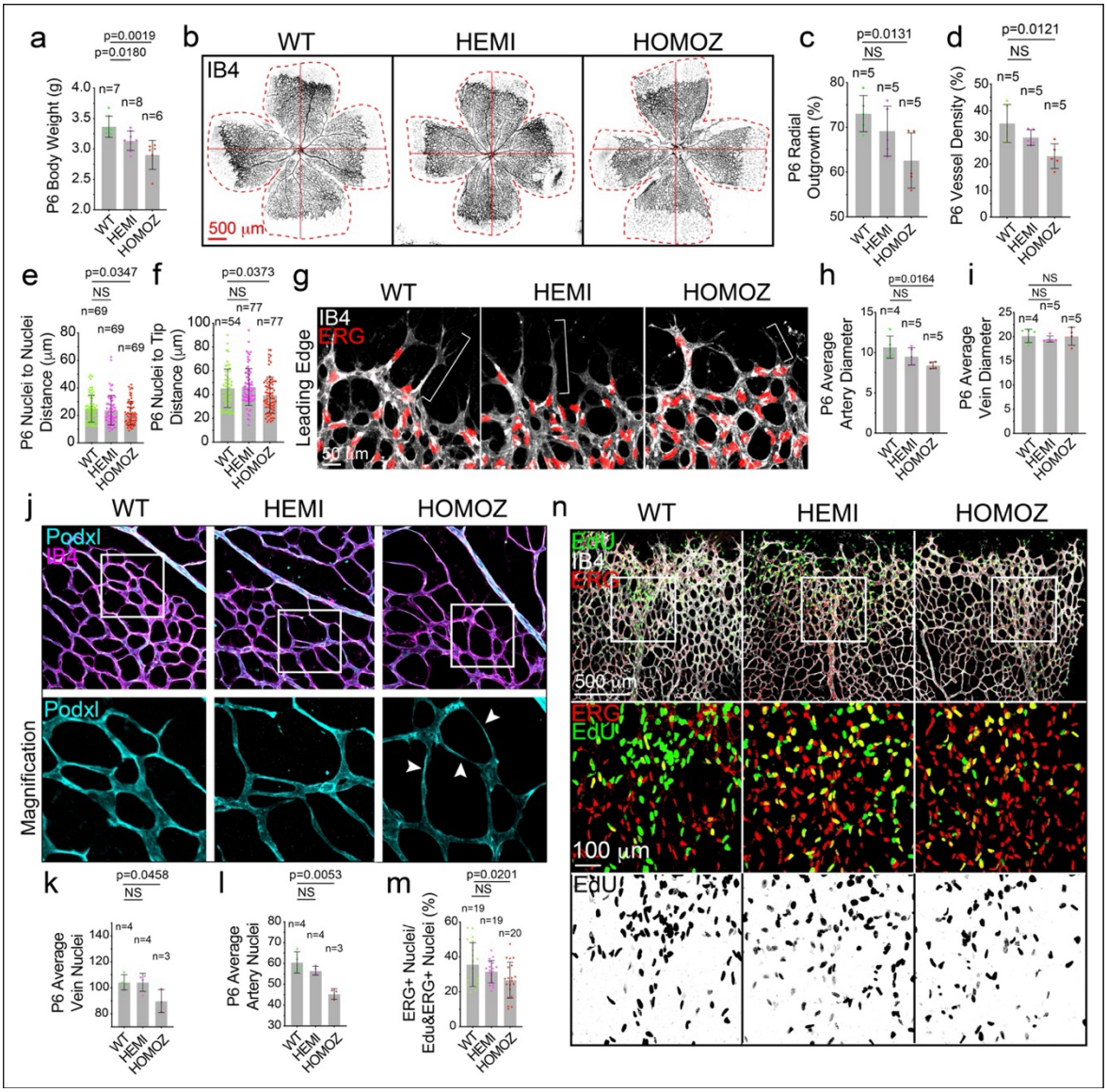

Figure 1 Progerin Expression Delays Retina Vascular Outgrowth in P6 Mice. a) Quantification of P6 pup body weight. b) Image representatives of P6 retinas. Dashed line denotes outline of retina. Quantification of c) radial outgrowth, d) P6 vessel density, e) nuclei to nuclei distance and f) nuclei to tip of leading-edge distance. n value = individual cells measured from 3 biological replicates per condition. g) Image representatives of P6 retina vascular leading edge. Brackets denote length between nuclei and endothelial cell protrusion tips. Quantification of h) P6 average artery diameter, and i) P6 average vein diameter j) Image representatives of arterial vessel density. Vessels are marked by IB4 and luminal marker podocalyxin (podxl). Quantification of k) P6 average vein nuclei number, l) P6 average artery nuclei number and m) ERG-positive nuclei by EdU and ERG positive nuclei. n) Image representatives of vessels marked with IB4, ERG (nuclei) and EdU (proliferation). In all figures box denotes area of magnification. a, c-f, and k-l quantifications N-value is of biological replicates. The average nuclei number, or vessel diameter, is calculated from multiple measurements along the length of primary arteries and veins.

vascular front and within the venous plexus, endothelial nuclei expressing the nuclear marker, ETS-related gene (ERG), were significantly closer in proximity in homozygotes than in littermate controls (**Figure 1e**). Additionally, projections at the leading edge were shorter with the nuclei to tip distance significantly decreased in homozygotes relative to controls (**Figure 1g**). In the maturing vascular plexus behind the vascular front, the lumen diameter of arteries, visualized by staining with the endothelial luminal marker Podocalyxin (Podxl), was significantly smaller than controls; this was not the case in veins (**Figure 1j-l**). Although arterial vessels were thinner, vessel perfusion with Sulfo-NHS-Biotin did not reveal a significant difference across groups at this stage (**Supplemental Figure 1d-e**).

EdU pulse and analysis at P6 was used to test if Progerin altered endothelial proliferation. We observed significantly fewer Edu/ERG+ proliferative endothelial cells as well as total endothelial cells in the veins and arteries of homozygotes compared to littermate controls (**Figure 1k-n**). Hence, nuclear defects in sprouting tips at the leading edge of the vasculature along with reduced proliferation in the vascular plexus and vessel thinning impaired retinal vascular development in homozygous P6 Progeric mice.

Lumen Collapse and Reduced Microvasculature Perfusion in 20-Week Progerin Homozygote Retinas

To determine how Progerin affected retina vasculature development over time, we analyzed mice at 10 and 20 weeks, prior to the average onset of death in homozygote LMNA G608G mice. Quantifications revealed that arterial lumen diameter remained reduced in 10-week-old homozygotes and worsened at 20-weeks in both arteries and veins **(Figure 2a-d, Supplemental Figure 2a-d**). Perfusion of capillaries with Sulfo-NHS-Biotin was significantly reduced in 20-week homozygous Progeric mice compared to controls (**Figure 2a-d**). In addition to reduced diameter, arteries and veins of homozygote retinas displayed a loss of smooth muscle cell coverage, marked by smooth muscle actin (**Fig 2a, Supplemental Figure 2e-f**).

To characterize how endothelial cells were affected by Progerin expression we probed for the endothelial junctional protein, VE-Cadherin (VECAD), endothelial luminal marker, Podxl, Collagen IV, and endothelial nuclei marker ERG. We did not observe any obvious changes in VECAD organization or Collagen IV intensity between genotypes, however, this staining revealed significantly thinner, and less dense, vessels of homozygotes. Staining with luminal marker Podxl also indicated vessel thinning as well as significantly greater vessel collapses (**Figure 2c-g, Supplemental Figure 2g-j**). Vessel collapses frequently occurred at sites where nuclei protruded into the lumen.

To understand the biochemical effects downstream of reduced perfusion, we isolated whole retinas and lysed them for western blotting (**Figure 2h-l**). Hypoxia-Inducible Factor-1a (HIF-1a) was increased in homozygous retinas, indicating greater incidence of hypoxia. We probed for endothelial nitric oxide synthase (eNOS) and phosphorylated-eNOS at serine 1177 to check for changes in vascular tone. We discovered markedly greater phosphorylated eNOS, suggesting a possible compensatory effect by activating eNOS to dilate vessels. Lastly, we probed for markers of DNA damage repair (H2a.x) and inflammation (NF-κB). For both markers, homozygous mice showed significant signs of increased DNA damage and inflammation.

In summary, the microvasculature is significantly impaired over the lifespan of homozygote Progerin mice with defects worsening over time. By 20-weeks, mice expressing Progerin have reduced retinal capillary perfusion and hallmarks of DNA damage, hypoxia, and inflammation.

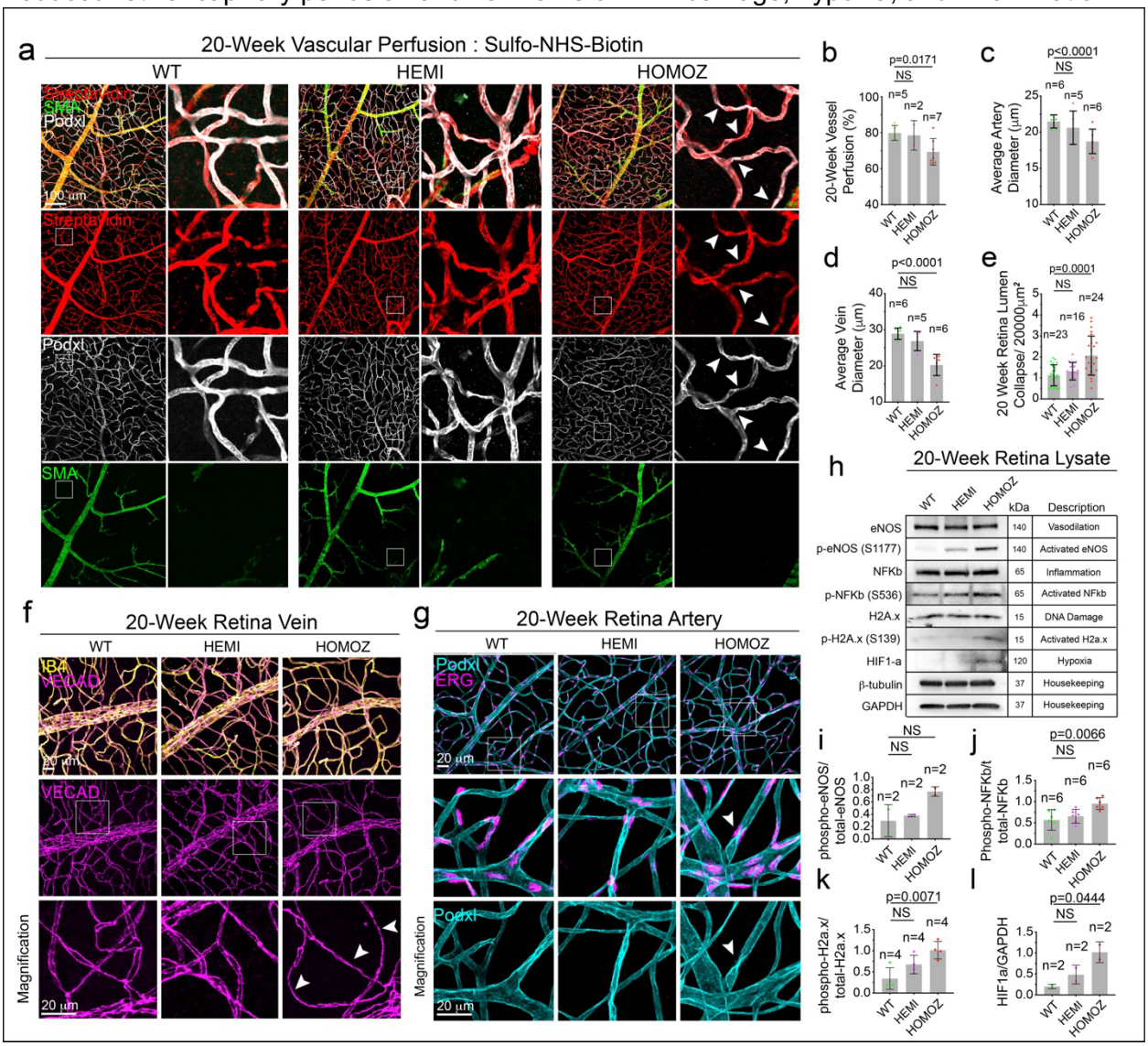

Figure 2. Microvasculature of 20-week Mice Expressing Progerin is Poorly Perfused. a) Image representatives of vessel perfusion with smooth muscle actin (SMA), podxl, and streptavidin (Sulfo-NHS-Biotin binding). Arrowheads indicate lumen collapse. Quantification of b) 20-week vessel perfusion (N = biological replicate), c) average artery diameter (N = biological replicate), d) average vein diameter (N = biological replicate), and e) lumen collapses by area (total mice quantified is 4 per condition). f) Image representatives of veins with VE-Cadherin (VECAD) and IB4. Arrowheads denote thin vessels. g) Image representatives of the artery with podocalyxin (podxl) and endothelial nuclei marker (ERG). Arrowheads denote lumen collapse. h) Western blotting of whole retina lysate for indicated proteins. Quantification of i) serine-1177 phosphorylated-eNOS by total eNOS, j) serine-536 phosphorylated NFKb by total NFKb, k) serine-139 phosphorylated H2A.x by total H2a.x and l) total HIF1a by total GAPDH. N= number of separate lysates. In all images box denotes area of magnification.

Cytoskeletal Defects in the Aortic Endothelium of 20-Week Mice Expressing Progerin

To address the mechanism of dysfunction, we investigated endothelial cells lining the aorta using en face imaging, which allows for a comprehensive view of endothelium in an intact flat layer and high-resolution imaging of protein and organellar localization. We analyzed mice at 10

weeks and 20 weeks at the inner curvature of the aortic arch, where endothelium is subject to disorganized flow. At 10-weeks of age, the homozygous Progeric aorta displayed similar SMC coverage compared to littermate controls, while the 20-week aorta displayed significant reduction of SMC and adipose coverage in homozygotes (**Figure 3a-d, Supplemental Figure 3a**), thus, we sought to investigate endothelium pre- and post- smooth muscle cell loss at 10 and 20 weeks respectively.

Nuclear lengths and widths of endothelium consistently trended shorter and wider in homozygotes at 10-weeks, however only at 20-weeks was this difference significant when compared with wildtype controls (**Figure 3e-h**). Nuclear positioning in the cell, measured by nuclei to plasma membrane (PM) distance and nuclei to nuclei distance, was significantly different for 20-week homozygote Progeric mice but not for 10-week mice relative to controls. Nuclei of 20-week homozygotes would cluster, quantified by nuclei-to-nuclei distance, and were significantly more likely to make contact with the plasma membrane when measured against control nuclei (**Figure 3i-l**). These findings led us to visualize Lamin-A/Progerin localization at the nucleus. We did not observe any loss of Lamin-A intensity across conditions, however, the localization of lamin-was concentrated and unevenly distributed across the nucleus in homozygote nuclei but not in wildtype control nuclei (**Supplemental Figure 3b**). Together, these data suggest that Progerin expressing endothelial cell nuclear shape and localization progressively worsen with time.

As nuclear shape and localization depend on cytoskeletal proteins, we next sought to compare cytoskeletal proteins, filamentous actin (F-actin) and vimentin, between conditions at 10 and 20 weeks. F-actin appeared less robust at the plasma membrane and less stress fibers were visible in the homozygote 10-week and 20-week mice than in control aortic endothelial cells (**Figure 3m, p**). We quantified f-actin stress fiber lengths and fibers were significantly shorter in homozygotes at 10 and 20 weeks compared to wildtype controls (**Figure 3n-o**). 20-week hemizygote stress fibers were also significantly shorter than controls suggesting the degree of expression determines severity of phenotype. The reduced actin at the membrane prompted us to check endothelial junctions and while the junctions appeared consistent, the membrane was less rounded, and the total perimeter was significantly longer in homozygotes against wildtype controls (**Supplemental Figure 3c-e**).

In addition to the actin cytoskeleton, we also investigated the intermediate filament, Vimentin. Vimentin is well-known to interface with the nucleus as well as at plasma membrane junctions and is reportedly decreased in Progeria (Song). Staining for Vimentin at 10-weeks and 20-weeks revealed significantly less density of Vimentin around the nucleus and an overall difference in organization in homozygotes compared to controls (**Figure 3q-t**). In total, endothelial specific cytoskeletal defects precede the loss of smooth muscle cell coverage, suggesting an endothelial specific origin.

Loss of perinuclear vimentin was particularly notable, as a recent case report demonstrated that mutation of vimentin (1160 T>C) can lead to a premature aging phenotype.[9] This observation suggested that vimentin disruption might represent a mechanistic link between Progeria and normal aging. To investigate this possibility, we analyzed aortae from 24-month-old wild-type mice and compared them with those from 4-month-old controls, assessing nuclear morphology,

F-actin, and vimentin organization. Endothelial cells from aged aortae exhibited significantly

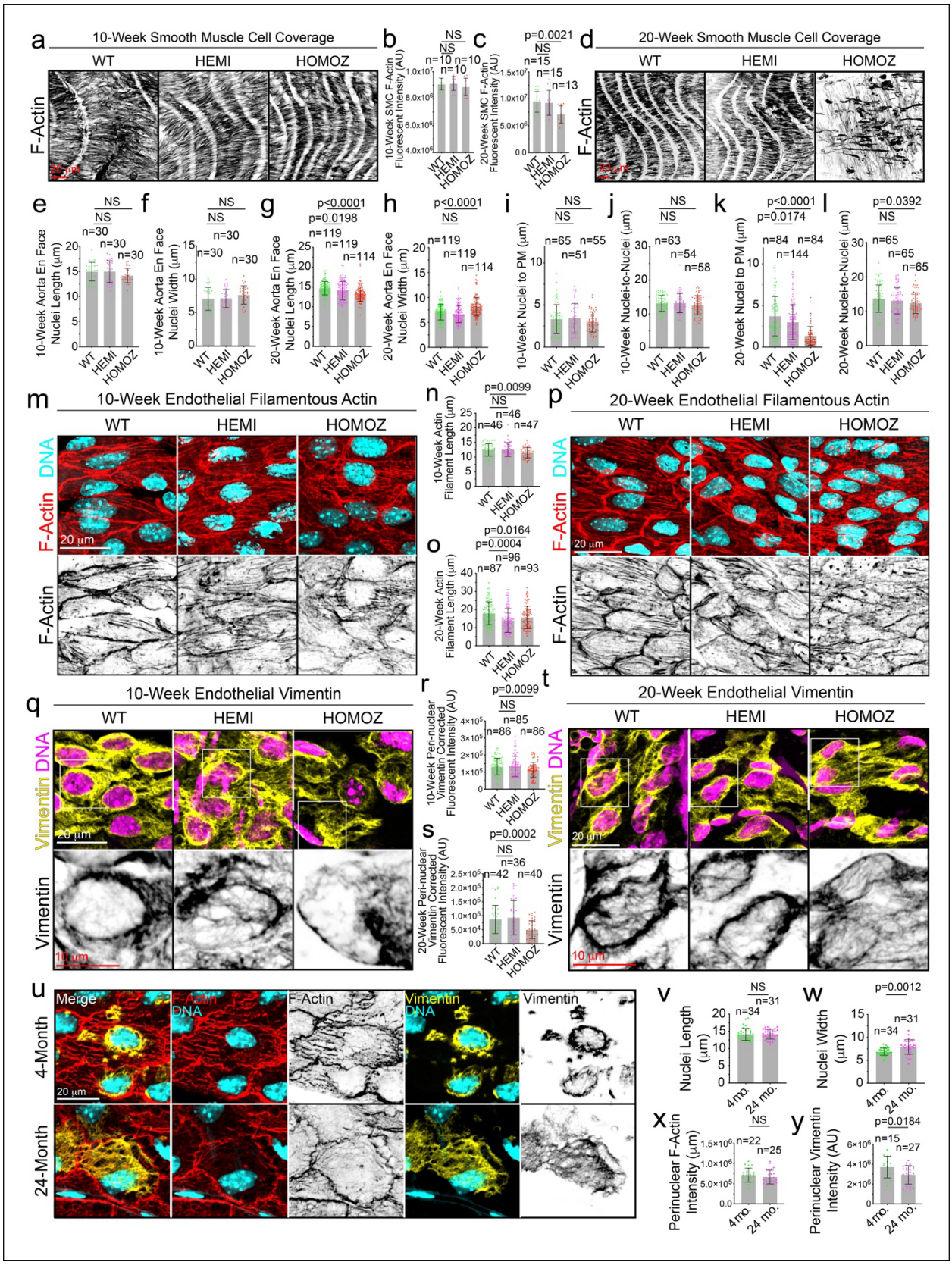

Figure 3. Progeric 10- and 20-week Aortic Endothelial Cells have Cytoskeletal Defects. a) Image representatives of 10-week aorta en face filamentous-actin (f-actin) of smooth muscle cell layer. Quantification of b) 10-week and c) 20-week f-actin intensity in smooth muscle cell layer. d) Image representatives of 20-week aorta en face f-actin of smooth muscle cell layer. Quantification of e) 10-week nuclear length, f) 10-week nuclear width, g) 20-week nuclear length, h) 20-week nuclear width, i) 10-week nuclei to plasma membrane (PM) distance, j) 10-week nuclei to nuclei distance, k) 20-week nuclei to plasma membrane distance, and l) 20-week nuclei to nuclei distance. For all quantification nuclei were quantified within inner aortic arch region. m) Image representatives of 10-week aorta en face inner curvature stained for f-actin (filamentous actin) and DNA. Quantification of n) actin filament length at 10pweeks and o) 20-weeks. p) Image representatives of 20-week aorta en face inner curvature stained for filamentous actin and DNA. q) 10-week aorta en face inner curvature stained for vimentin and DNA. Box denotes area of magnification. Quantification of r) perinuclear vimentin fluorescent intensity at 10-weeks and s) 20-weeks. t) 20-week aorta en face inner curvature stained for vimentin and DNA. Box denotes area of magnification. u) Image representatives of wildtype 4 month old mice and 24 month old mice for indicated stainings. Quantification of 4- and 24-month v) nuclear length, w) nuclear width, x) perinuclear f-actin, and y) perinuclear vimentin. For all quantification a minimum of 3 biological replicates were measured.

wider nuclei compared to those from young mice, indicating that nuclear shape changes occur during normal aging. In addition, aged endothelial cells displayed significantly reduced perinuclear vimentin and a modest, though not statistically significant, reduction in perinuclear actin relative to younger controls (Figure 3u–y). Together, these findings identify a potential mechanistic connection between Progeria and normal aging through alterations at the nuclear–cytoskeletal interface involving vimentin, warranting further investigation.

Ex Vivo Vessel Sprouting Determines Cell Autonomous Nature of Endothelial Defects

To uncover the endothelial cell specific effects of nucleo-cytoskeletal disruption by Progerin expression we isolated brain endothelial cells from homozygous, hemizygous and wildtype littermates at P6 and grew vessels ex vivo using microcarrier beads (**Figure 4a**). This assay allows for studying sprouting angiogenesis of endothelium in isolation. We used the previously described mouse ERG antibody to quantify percent of endothelial cells per bead between conditions and observed no significant difference (**Figure 4b-c**). WT, hemi- and homozygous vessels formed similar numbers of vessels from each bead, but they were significantly shorter in homozygotes than controls (**Figure 4d-e**). Consistent with in vivo observations, fewer vessels grown from homozygote mutants were lumenized compared to hemizygous and wildtype (**Figure 4f-g**). In homozygotes we observed nuclei central to the vessel where lumen formation would occur. Additionally, nucleosomes were observed in hemizygotes and homozygotes (**Figure 4g**).

For lumen formation to occur, endothelial must undergo significant shape change by relocating peripherally and flattening. Homozygous nuclei failed to relocate and change shape for this process to occur. Homozygote nuclei size were larger than controls, with significantly greater length and width (**Figure 4k-l**). Homozygous nuclei were significantly more clustered together compared to controls (**Figure 4m**). At the sprout tips, the distance between the nuclei and the tip of the sprout was significantly shorter in homozygotes (**Figure 4j**), as observed in the P6 retinas. These results show that Progerin impacts endothelium independently of influence from surrounding blood and tissue.

Aberrant Nuclear Dynamism and Cytoskeletal Dysfunction of Progerin-Expressing Endothelial Cells

To determine if our observations in the mouse model translate to humans, we used a fluorescently tagged Progerin lentivirus that was transduced into human umbilical vein endothelial cells (HUVECs) by lentivirus. Nuclear localized sequence (NLS)-GFP and full-length

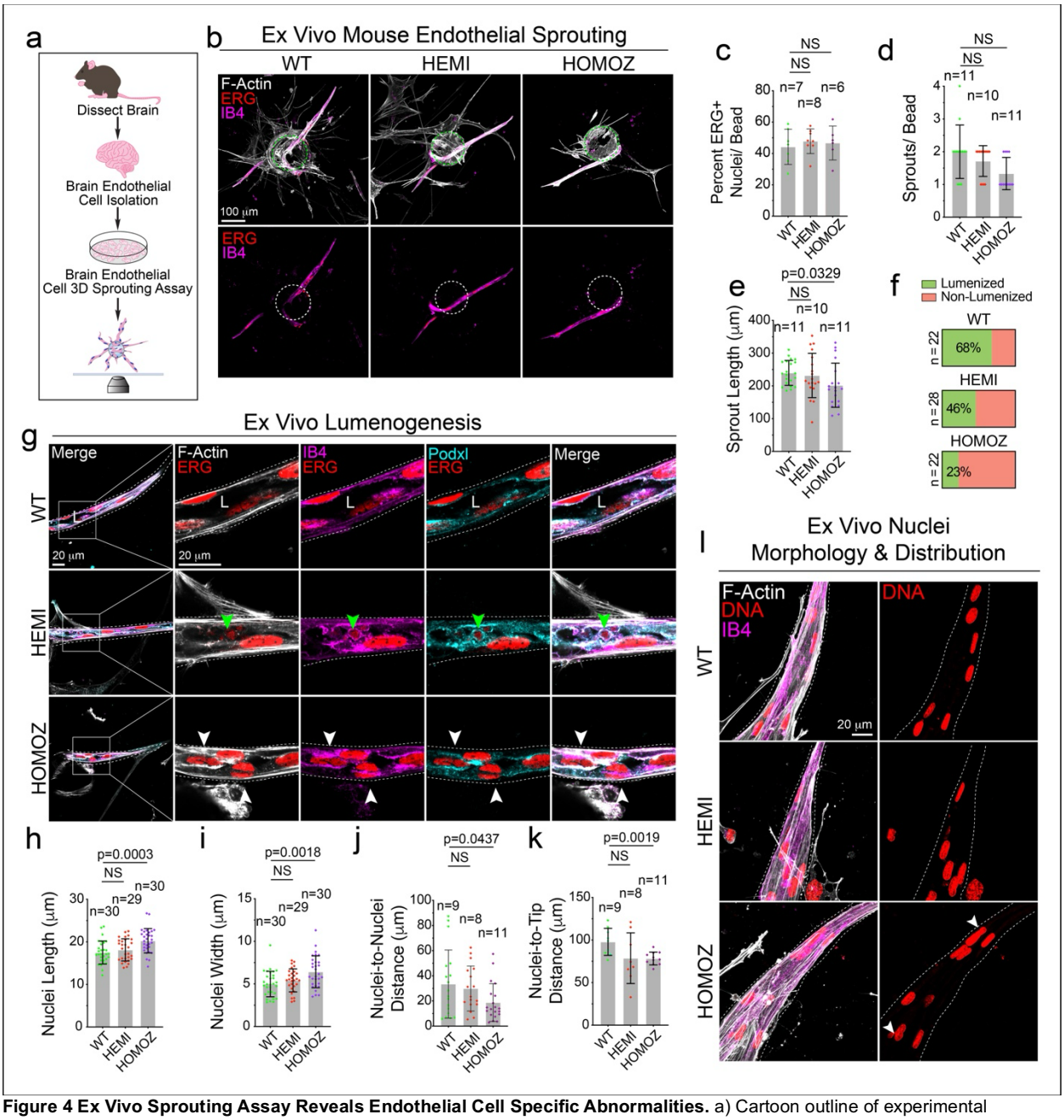

Figure 4 Ex Vivo Sprouting Assay Reveals Endothelial Cell Specific Abnormalities. a) Cartoon outline of experimental procedure. b) 20x image representatives of ex vivo sprouting assay vessel morphology. Dashed circle denotes microcarrier bead. Quantification of c) ERG-positive nuclei per bead d) sprout number per bead, e) sprout length and f) percent of lumenized vessels. g) 60x z-slice image representatives of vessel lumen formation. White arrowheads denote abnormally localized nuclei. Green arrowhead denotes nucleosome. Quantification of h) nuclei length, i) nuclei width, j) nuclei to nuclei distance, and k) nuclei to tip distance. l) 60x z-projection image representatives of nuclei morphology. In all panels dashed lines outline sprouts.

Lamin-A (LMNA)-GFP lentivirus were used as controls. With this tool, we analyzed how Progerin-expression alters human endothelial cell sprouting. Lentivirus was titrated to allow for mosaic Progerin expression in a subset of all cells, to allow for side by side comparison of Progeric and healthy nuclei in the same vessel. To measure the potential of transduced cells to invade sprouts, we quantified the number of GFP-positive nuclei in sprouts against the total number of GFP-positive cells on the bead and in sprouts. More than 35% of NLS or Lamin-A-GFP expressing cells were localized in sprouts, while only 10% of Progerin- GFP+ cells were

located in sprouts (**Figure 5a-b**), demonstrating a disadvantage of Progeric cells to migrate into sprouts compared to controls. Although rare, when present in the tip position the GFP-Progerin expressing nuclei were located closer to the leading edge of the tip cell than the controls (**Figure 5c-d**). Nuclear length and width were increased in Progerin GFP+ cells compared to NLS and Lamin-A-GFP controls (**Figure 5e-g**). Protrusion of Progerin-GFP nuclei into the lumen reduced lumen formation and diameter compared with the surrounding uninfected nuclei (**Figure 5e, Supplemental Figure 4a-c**).

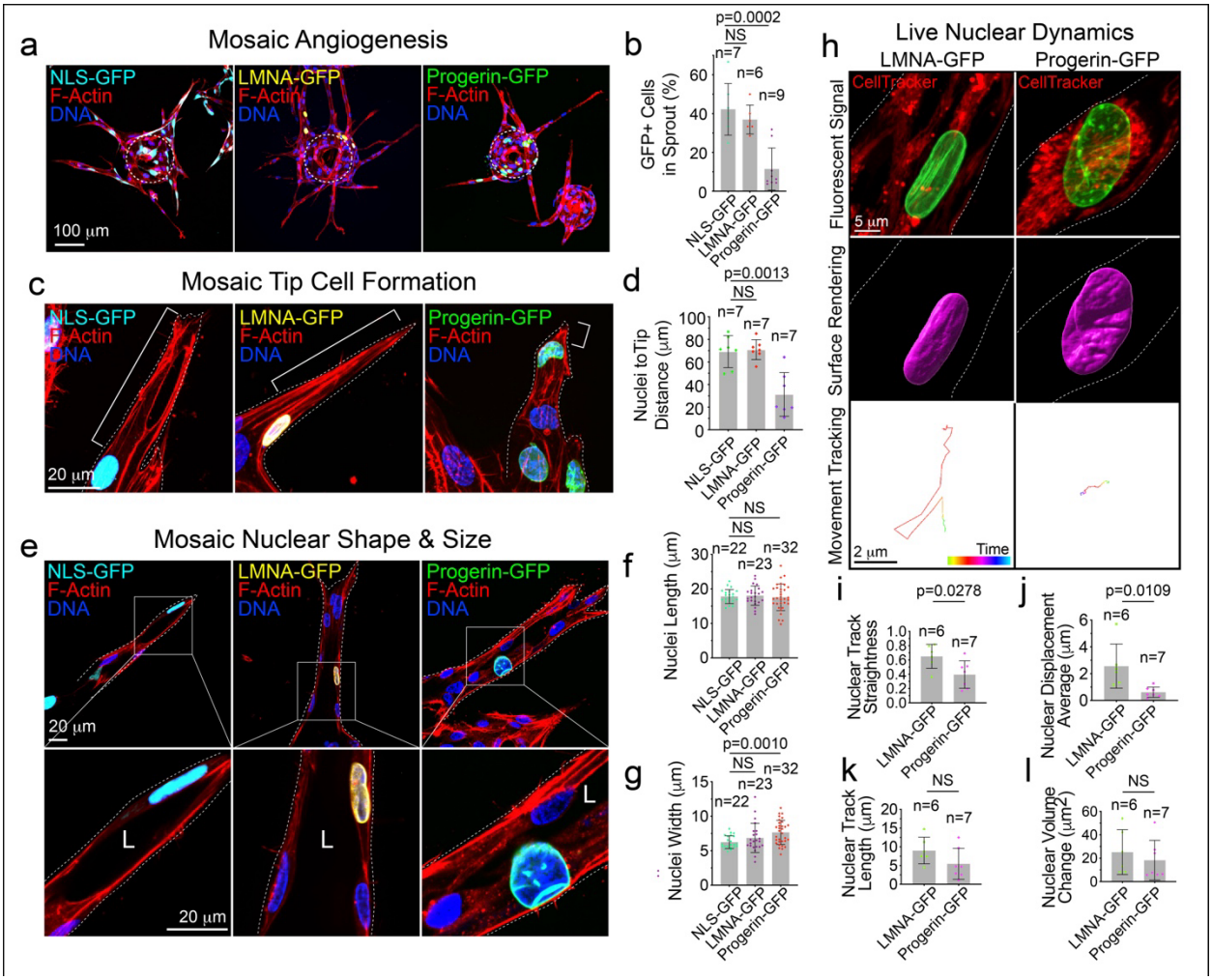

Figure 5. Mosaic Progerin Expression in Human Vessels Reveals Abnormal Nuclear Dynamism. a) 20x image representatives of mosaic nuclear localized sequence (NLS)-GFP, Lamin-A (LMNA)-GFP and Progerin-GFP sprouting assays. Dashed circle denotes bead. b) Quantification of GFP+ cells per sprout by total GFP+ cells on bead and in sprouts. N=number of beads. c) Z-projection image representatives of indicated condition tip cells. Bracket denotes measurement. d) Quantification of nuclei to tip distance. e) Z-slice image representatives of indicated conditions lumen development. Box denotes area of magnification, L denotes lumen. Quantification of f) nuclear length and g) nuclear width. h) Z-projection image stills of live imaged nuclei. Middle panels are nuclei surface rendering and bottom panels are of live imaging tracks. Quantification of i) nuclear track straightness, j) nuclear displacement average, k) nuclear track length, and l) nuclear volume change. N=number of nuclei live imaged.

We live imaged full-length Lamin-A-GFP and Progerin-GFP nuclei over 4 hours of lumen formation and observed nuclei which oscillated in place with poor directionality compared with Lamin-A nuclei (**Supplemental Movie 1**). Over multiple imaging sessions, we quantified nuclear track straightness and average nuclear displacement over time, both of which were significantly different compared to Lamin-A nuclei (**Figure 5h-j**). The length of the tracks was not significant between conditions, suggesting that nuclei moved a comparable amount however not in a consistent direction. Lastly, we quantified nuclear volume as a control to ensure that nuclei remained healthy, and did not shrink, over the course of imaging (**Figure 5k-l**).

Impaired nuclear mobility may be indictive a functional defect within the cytoskeleton, we tested whether cytoskeletal protein activity was altered by Progerin expression. We probed Progerin, and NLS-control lysate for cytoskeletal activity indicators, including a focal adhesion regulator (focal adhesion kinase (FAK), actin turnover (cofilin), and intermediate filament protein (Vimentin). Phosphorylation levels of FAK, cofilin, and vimentin were significantly higher for Progerin expressing cells; although FAK phosphorylation was higher, total FAK was significantly elevated (**Supplemental Figure 4d-**h). These results suggest that turnover of cytoskeletal proteins is higher in Progerin expressing cells.

Progerin Expression Impairs Endothelial Nucleoskeletal-Cytoskeletal Interface

To understand how Progerin impacts the nucleoskeletal-cytoskeletal interface, we imaged HUVECs transduced with Progerin-GFP or control LMNA-GFP. Because Vimentin antibodies did not give us high-quality immunostaining, we probed for Vimentin by co-transducing with Vimentin-mCherry and for filamentous (f-)actin by immunolabeling. Both f-actin and Vimentin localized abnormally in Progerin-GFP nuclei compared with control LMNA-GFP nuclei, with significantly reduced perinuclear localization that affected Vimentin most severely (**Figure 6a-c**). This phenotype was consistent between 2D and 3D assays (**Supplemental Figure 4d**).

LINC complex proteins Nesprin1-3 and Sun1 form the transmembrane interface between Lamin-A and the cytoskeleton. Previous reports suggest that Sun1 abundance in the nuclear membrane is increased with Progerin expression, indeed we observed higher Sun1 protein signal in cells expressing Progerin (**Figure 6d-e**).[7,8] Given the increased levels of Sun1 we further investigated other LINC complex proteins and nuclear cytoskeletal proteins by isolating nuclear and cytoplasmic fractions. With western blotting we probed for Sun1, Nesprin1, Nesprin2, Nesprin3, Vimentin, b-actin, b-tubulin, GAPDH and Nup98 (**Figure 6f**). Nup98 signal was only detected in the nuclear fraction, while b-tubulin and GAPDH were only detected in the cytosolic fraction as expected (**Figure 6f**). Sun1 was only detected in the nuclear fraction and consistently higher in Progerin expressing cell nuclear fractions compared to controls (**Figure 6g**). Nesprin1 and 2 were detected in both cytosolic and nuclear fractions, with enrichment in control nuclear fractions compared to the cytosolic ones. Nuclear fractions in Progerin expressing cells showed a decrease in Nesprin1 and 2 immunoreactivity, however, only Nesprin1 nuclear fractions for Progerin expressing cells was significantly different between conditions (**Figure 6h-j**). The higher kilodalton band of Nesprin3 was reduced in Progerin nuclear fractions, but its levels were not significantly different between groups (**Figure 6j**). There were no quantifiable differences in b-actin, or a/b-tubulin between nuclear and cytoplasmic

fractions, but Vimentin was significantly less detectable in the nuclear fraction of Progerin expressing cells (**Figure 6k-m**).

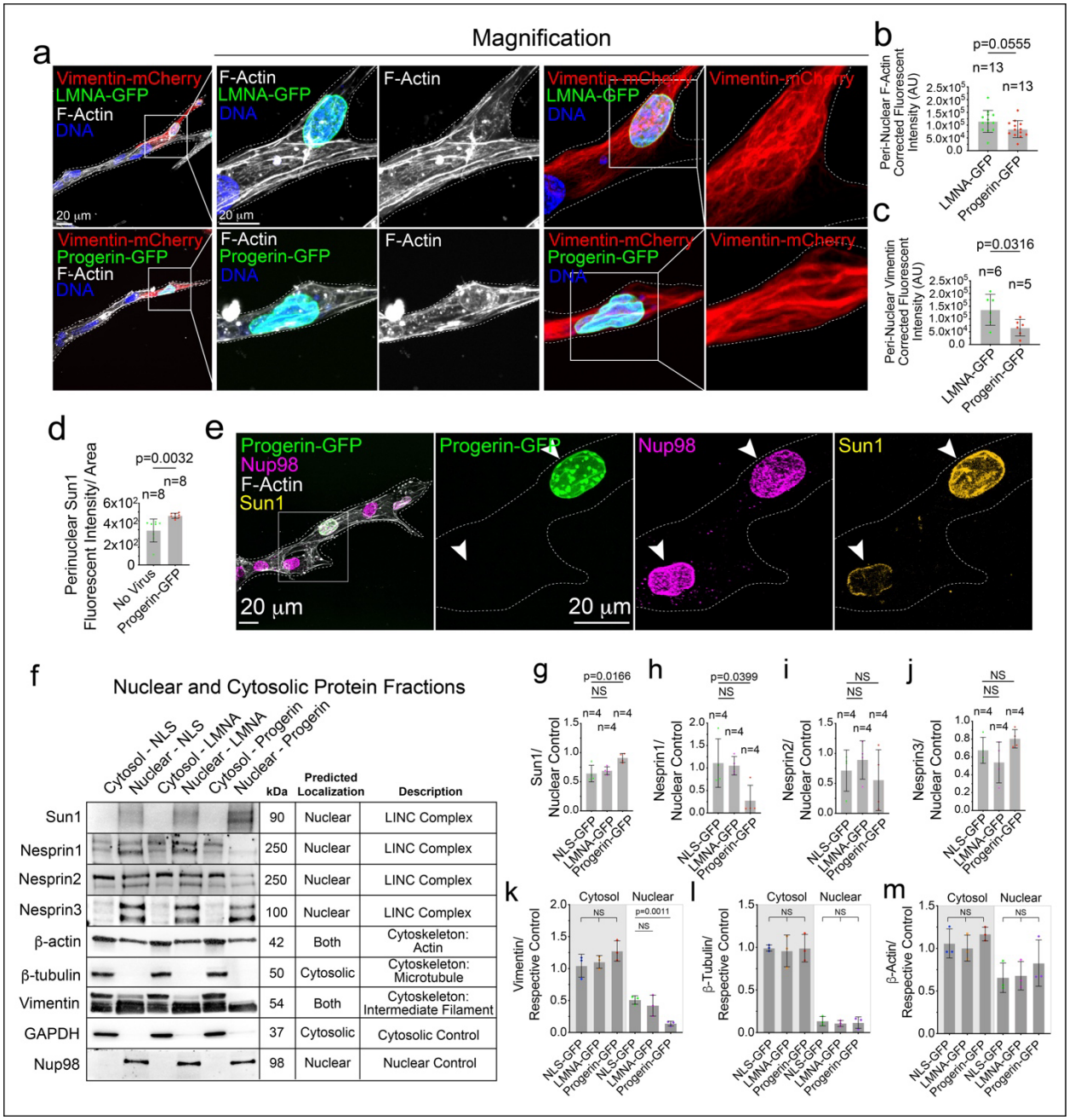

Figure 6. Endothelial Cell Nuclear Membrane Makeup is Altered with Progerin Expression. a) 60x z-projection image representatives of Lamin-A (top panels) and Progerin (bottom panels) with f-actin and Vimentin-mCherry. Quantification of b) perinuclear fluorescent intensity of f-actin and c) perinuclear fluorescent intensity of Vimentin-mCherry. d) Quantification of Sun1 intensity in Progerin-negative and Progerin-positive cells. e) Z-projection image representatives of Progerin-GFP expression and staining for Sun1 abundance. f) Western blotting of nuclear and cytoplasmic fractions for described LINC complex proteins and cytoskeletal proteins. The first fraction is nuclear localized GFP expressing cells, second is full length Lamin-A expressing cells and last is Progerin expressing cells. g-m) Quantification of western blotting repeats. Respective controls refers to either the cytosolic contrl (GAPDH) or nuclear control (Nup98). In probes which resulted in multiple bands, all bands were quantified, with the exception of Vimentin (top band only).

To more concretely determine Nesprin binding to the nuclear membrane, we electroporated the fluorescently tagged (Emerald) Nesprin-3. Nesprin-3 was ideal given its smaller size compared with the giant Nesprin 1 and 2 isoforms. We observed a slight decrease in Nesprin3 immunofluorescence in Progerin expressing cells and an increase of vesicular Nesprin3 (**Supplemental Figure 4e-g**). These results, coupled with the nuclear fractions suggests that Nesprin's are most likely still present in the nuclear membrane, however, they are less abundant and mislocalized compared with Lamin-A expressing cells. Indeed, the re-localization of Nesprins has been previously reported (Chen). In closing, LINC complex proteins are disrupted by Progerin expression and subsequently the interface with cytoskeletal proteins is severely diminished.

Inhibition of Actin Branching or Vimentin Activation Cause Abnormal Nuclear Shape and DNA Damage

To understand which cytoskeletal proteins are required for nuclear movement during sprouting angiogenesis we used inhibitors to reduce functionality of actin (Ck-666, arp2/3 inhibitor), vimentin (Five1 inhibitor), and microtubules (nocodazole, microtubule stabilizer). Vessels were treated pre-lumization after 3 days of growth and challenged to continue growing for an additional 3 days (**Figure 7a**). Microtubule stabilization did not result in aberrantly misshaped nuclei. However, nuclei did adopt a 2D planar cell nuclear phenotype which were extremely flat and wide compared to all other conditions (**Figure 7b-c, Supplemental Figure 5a**). Vimentin inhibitor and actin branching inhibitor both resulted in significantly misshapen nuclei. In both conditions, nuclei were significantly shorter and wider, with reduced sphericity (closeness a 3D object resembles a sphere) and nuclear height compared to DMSO (**Figure 7a-c, Supplemental Figure 5b-c**).

Nuclei to tip distance was significantly shorter for Vimentin and Microtubule disruption but less so for actin disruption (**Figure 7d**). Sprouting parameters such as sprouts per bead, sprout length and percentage of lumenized sprouts were all significantly different for each inhibitor, however actin branching inhibited sprouts were longer and had more sprouts per bead compared with the other inhibitors (**Figure 7e-g**).

Imaging of nuclear proteins Lamin-A, Sun1 and Nup98 revealed that vimentin and Arp2/3 inhibitors induced nuclear membrane invaginations (**Figure 7h**). Severe nuclear membrane shape changes is associated with DNA damage.[14,28,31] Thus, we lysed inhibitor-treated HUVECs and probed for DNA damage marker H2a.x (**Figure 7i**). Expression of H2a.x was significantly increased for both vimentin and Arp2/3 inhibitor lysate compared to control or microtubule stabilized cell lysate (**Figure 7j**). We also probed lysate for Vimentin, phosphorylated-Vimentin, and a/b-tubulin to ensure inhibitors were working effectively. We confirmed hyperphosphorylation of Vimentin in Five1 treated lysate and confirmed microtubule stabilization does not reduce total α/β-tubulin (**Figure 7i-l**). Together, these results indicate that actin and vimentin are required to maintain nuclear shape whereas microtubule stabilization altered 3D polarity and subsequent programming for lumen hollowing.

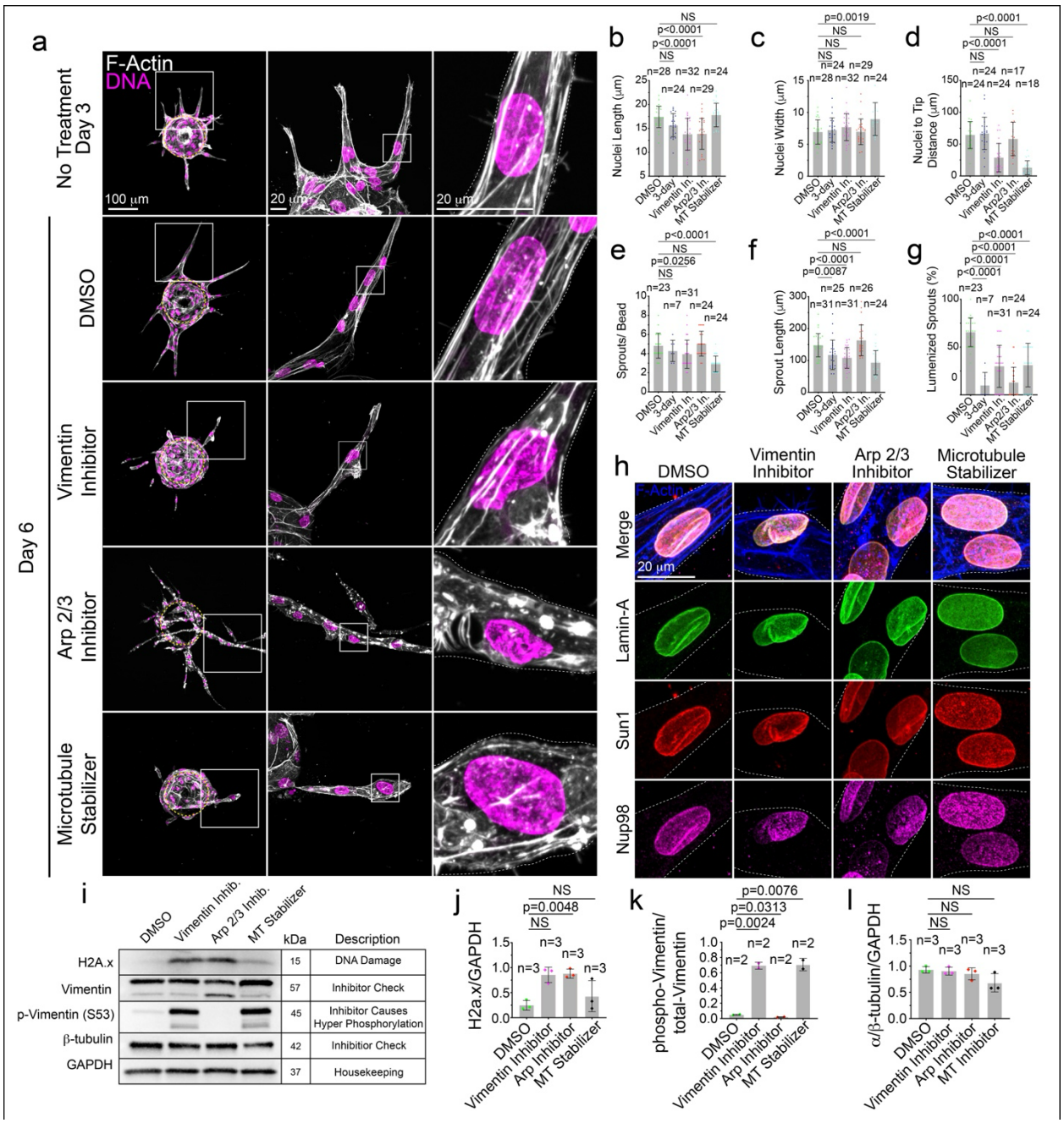

Figure 7. Vimentin and Actin Inhibition Alters Nuclear Shape and Induces DNA Damage. a) Image representatives of vessels before and after inhibitor treatment. DMSO = vehicle, Vimentin inhibitor = Five1, arp2/3 inhibitor/ actin disruption = CK-666, and Microtubule stabilizer = nocodazole. Column one is 20x vessel morphology, column two is z-projection of 60x morphology, and third column is magnification. Box denotes area of magnification. Quantification of b) sprouts per bead, c) vessel sprout length, d) percentage of lumenized sprouts, e) nuclei to tip distance, f) nuclear length relative to vessel length, and g) nuclear width. h) Z-projected image representatives of inhibitor treated nuclei stained for Lamin-A (green), Sun1 (red), and nuclear protein localized Nup98 (magenta). i) Western blotting for indicated proteins. j-l) Quantification of western blotting repeats for indicated proteins.

Loss of LINC Complex Proteins Results in Nuclear Mislocalization, Albeit Not as Severe as Progerin Expression

To determine if disruption of the LINC complex is sufficient to induce endothelial cell nuclear abnormalities we investigated depletion of individual LINC complex components. We used a

mosaic assay in which siRNA treated cells were marked with Cell Tracker and combined with untreated cells in a 50:50 ratio. Knockdowns were achieved by electroporation and confirmed with western blotting (**Supplemental Figure 6a-j**). All mosaic knockdown vessels formed similar

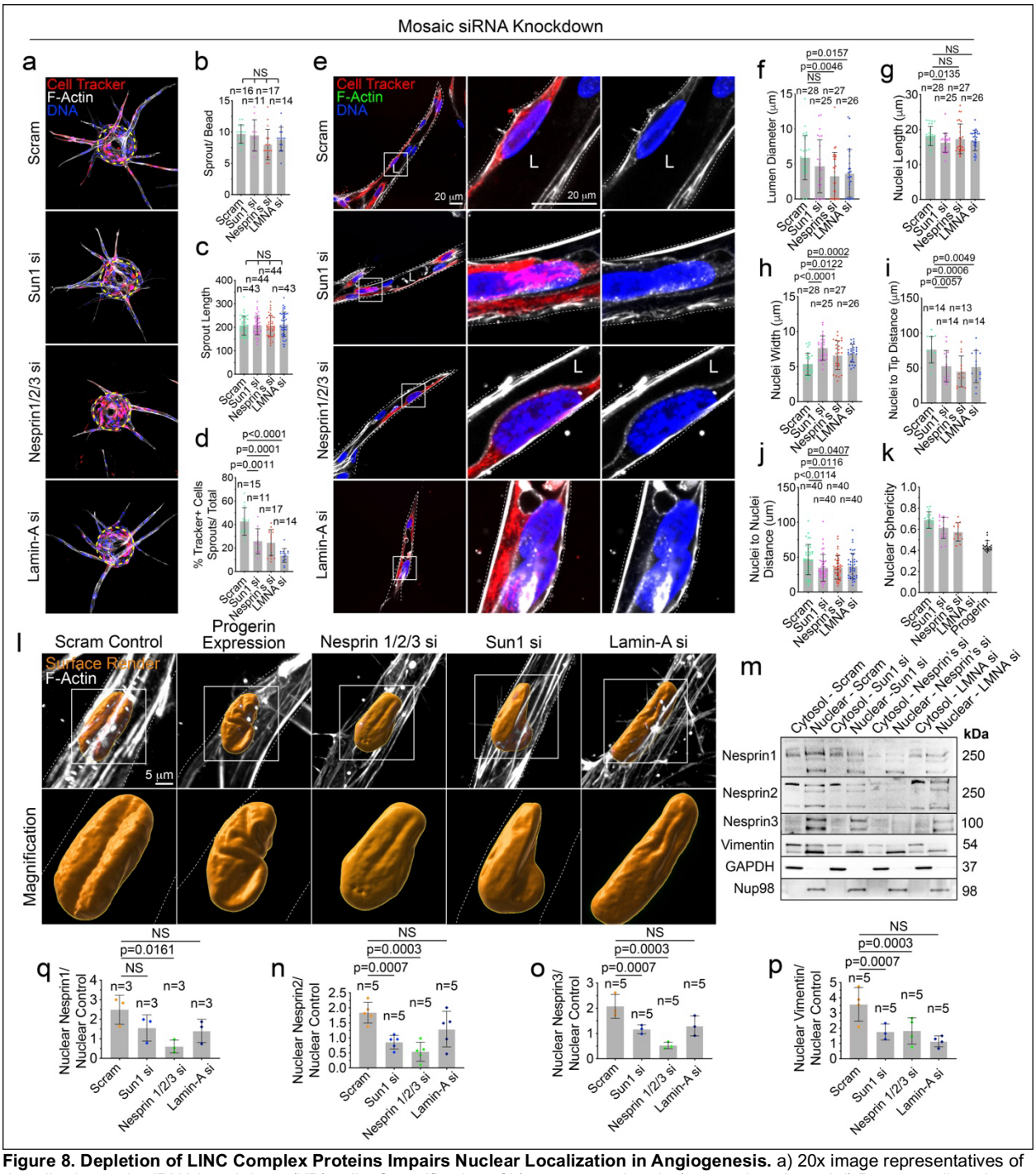

Figure 8. Depletion of LINC Complex Proteins Impairs Nuclear Localization in Angiogenesis. a) 20x image representatives of described mosaic siRNA knockdown (KD) cells. Quantification of b) sprouts per bead, c) sprout length, and d) Percent cell tracker-positive cells in sprouts by total cell tracker-positive cells on the bead and sprouts. e) 60x z-slice image representatives of described mosaic siRNA treated vessels. Quantification of f) lumen diameter, g) nuclei length, h) nuclei width, i) nuclei to tip distance j) nuclei to nuclei distance, and k) nuclear sphericity. l) Image representatives of Lamin-a surface rendering utilized for nuclear sphericity quantification. m) Western blotting for nuclear and cytosolic fractions of described siRNA knockdown cells n-l) Quantification of western blotting repeats. For all figures L denotes lumen and box represents area of magnification.

numbers of sprouts per bead and the length of the sprouts was similar between scrambled and other siRNA conditions (**Figure 8a-c**). However, Cell Tracker-positive cells in sprouts were significantly reduced in Sun1, Nesprin 1/2/3, and Lamin-A knockdown conditions (**Figure 8d**), indicating that LINC complex interruption reduced the ability of cells to move from the beads into the sprouts. Furthermore, consistent with all previous experiments, nuclei in knockdown cells were wider and obstructed lumen formation when compared to scramble control (**Figure 8e-h**). Tip cell projections were shorter, nuclei clustered, and nuclear sphericity was significantly altered by knockdown of Sun1 (**Figure 8i-k**). When compared with Progeric nuclear shape, Progerin-expressing cells were significantly more misshapen compared with LINC complex protein knockdown cells (**Figure 8l**). This is consistent with previous reports which indicate Progerin expression has a significantly greater negative effect on nuclei than Lamin-A depletion.[13,23]

To supplement the siRNA knockdown of all three Nesprins, we also used the readily available KASH binding protein (mCherry-KASH-DN) as a dominant negative to analyze depletion of all Nesprin binding and identified nuclear defects comparable to those observed with siRNA. Nuclear localization and shape, lumen hollowing, and tip cell formation were all significantly impaired (**Supplemental Figure 6k-q**).

Lastly, we sought to determine how individual knockdowns of LINC complex proteins effected abundance of other LINC complex proteins. We knocked down Sun1, all three Nesprins, and Lamin-A and fractioned the nuclei to measure abundance in the nuclear membrane. Sun knockdown significantly reduced Nesprin abundance compared to controls, however Lamin-A knockdown reduced Nespin coverage but this was not statistically significant relative to controls. For all knockdowns Vimentin coverage was significantly reduced (**Figure 8m-p**). These findings indicate that Nesprin is dependent on Sun for integrating into the nuclear membrane. Loss of any LINC complex protein alters Vimentin coverage, demonstrating that all components are required for interfacing. Finally, loss of Lamin A exerts a less pronounced effect on Nesprin and SUN protein abundance compared with Progerin expression, suggesting that Progerin more substantially alters nuclear membrane composition.

Patient Stem Cell Derived Endothelial Sprouting Assay is Partially Rescued by Progerinin Treatment

To test treatment options specific to endothelial improvement in patients with Progeria, we used induced pluripotent stem cells (iPSCs) from a Progeria patient, and the patient's unaffected parent's iPSC's for a control. We differentiated iPSCs to endothelial cells and challenged vessels to grow in vitro (**Figure 9a**). We stained vessel sprouts for endothelial specific VE-Cadherin to confirm cell-type identity, greater than 85% of cells were endothelial specific in both patient and parent (**Figure 9b-c**). Sprout number per bead and sprout length were similar between parent and patient (**Figure 9d-e**). The number of nuclei per sprout was significantly less in patient vessels compared with parent vessels (**Figure 9f**). Patient nuclei were significantly wider, shorter, and less spherical than parent nuclei (**Figure 9g-i**). Lumen formation was significantly impaired in patient sprouts relative to the parents (**Figure 9j-l**). The distance between nuclei and from the nuclei to the tip of the sprout were both significantly lower in patient vessels than parent vessels (Figure 9m-o). Finally, Vimentin perinuclear localization was

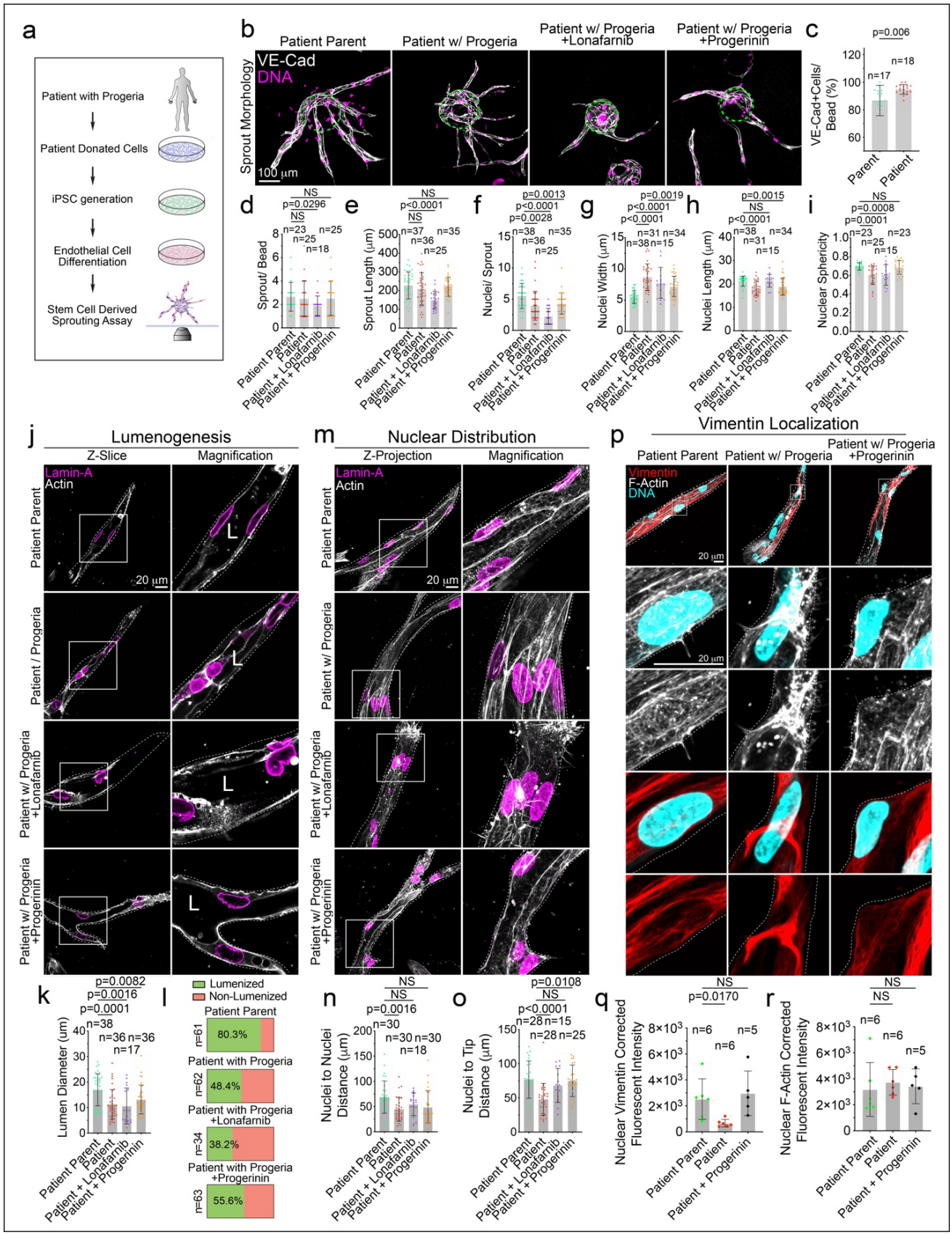
a
Patient with Progeria
Patient Donated Cells
iPSC generation
Endothelial Cell Differentiation
Stem Cell Derived Sprouting Assay
b
Patient Parent
Patient w/ Progeria
Patient w/ Progeria +Lonafarnib
Patient w/ Progeria +Progerinin
Sprout Morphology
VE-Cad
DNA
100 µm
c
p=0.006
VE-Cad+Cells/ Bead (%)
Parent
Patient
d
Sprout/ Bead
e
Sprout Length (µm)
f
Nuclei/ Sprout
g
Nuclei Width (µm)
h
Nuclei Length (µm)
i
Nuclear Sphericity
Patient Parent
Patient
Patient + Lonafarnib
Patient + Progerinin
j
Lumenogenesis
Z-Slice
Magnification
Lamin-A
Actin
20 µm
L
Patient Parent
Patient / Progeria
Patient w/ Progeria +Lonafarnib
Patient w/ Progeria +Progerinin
k
Lumen Diameter (µm)
l
Lumenized
Non-Lumenized
Patient Parent
Patient with Progeria
Patient with Progeria +Lonafarnib
Patient with Progeria +Progerinin
80.3%
48.4%
38.2%
55.6%
n=61
n=62
n=34
n=63
m
Nuclear Distribution
Z-Projection
Magnification
n
Nuclei to Nuclei Distance (µm)
o
Nuclei to Tip Distance (µm)
p
Vimentin Localization
Vimentin
F-Actin
DNA
q
Nuclear Vimentin Corrected Fluorescent Intensity
r
Nuclear F-Actin Corrected Fluorescent Intensity

Figure 9. Patient Stem Cell Derived Sprouting Angiogenesis Assay and Rescue. a) Cartoon illustrating experimental protocol. b) 20x image representatives of stem cell derived sprouting angiogenesis assay. Dashed line denotes bead. Quantification of c) VE-Cadherin (VE-Cad) positive cells per bead for parent (control) and patient cells, d) sprout number per bead. N=number of beads, e) sprout length. N=number of vessels, f) nuclei per sprout, n=number of vessels. g) nuclear width, h) nuclear length, and i) nuclear sphericity. j) Z-slice image representatives illustrating lumen formation. L denotes lumen. Quantification of k) lumen diameter. N=number of vessels, and l) percent lumenized vessels. N=number of vessels. m) Z-projection image representatives illustrating nuclear localization. Quantification of n) nuclei to nuclei distance and o) nuclei to tip distance. p) Image representatives of F-actin and vimentin in patient-derived vessels. Arrowheads denote nuclear membrane interface. Quantification of q) nuclear vimentin and r) nuclear f-actin.

significantly reduced in patient vessels (**Figure 9p-q**). There was no quantifiable difference in perinuclear filamentous actin (**Figure 9r**). We again observe a consistent endothelial cell phenotype in patient Progerin expressing cells.

We tested effects of the farnesylation inhibitor Lonafarnib, which is the only approved therapy for Progeria. We also tested a new drug known as Progerinin, which binds to the C-terminal Progerin domain and inhibits Progerin- Lamin-A binding while sparing wildtype Lamin-A.[20] We tested the effects of Lonafarnib and Progerinin treatment on nuclear Lamin-A abundance and observed a significant decrease in nuclear Lamin-A for Lonafarnib fractions but not for Progerinin fractions, compared with vehicle-control fractions (**Supplemental Figure 7a-d**). However, GFP-Progerinin expressing cells treated with Progerinin showed a decrease in nuclear GFP compared to untreated fractions (**Supplemental Figure 7e-f**). These results suggest that Lonafarnib reduces Lamin-A nuclear abundance and Progerinin effectively targets nuclear Progerin and not Lamin-A.

Lonafarnib treatment significantly improved nuclear length for the patient compared to the parent, but the treatment was detrimental to vessel development. Vessels treated with lonafarnib were significantly shorter with less nuclei per sprout and significantly impaired lumen formation compared to patient and parent vessels (**Figure 9d-l**). Progerinin, however, improved multiple sprouting parameters without any negative effect on development. Progerinin improved nuclear sphericity, lumen formation, nuclei to tip distance and nuclei to nuclei distance as there were either no significant differences or a reduced significant difference compared with parent vessels (**Figure 9f, j-o**). Perinuclear Vimentin localization was restored in Progerinin treated vessels as measured by fluorescent intensity as well as in nuclear fractions (**Figure 9p-q, Supplemental Figure 7g-h**).

Discussion

In this study, we propose Progerin expression impairs endothelial nuclear flattening and lumen hollowing in the microvasculature. Our findings indicate that this phenotype arises from a severely compromised nuclear-cytoskeletal interface and subsequent reduced nuclear re-shaping and mobility. Unlike prior studies that have focused on the macrovasculature of children with Progeria, the present study provides insight into the endothelial-specific effects of Progerin expression, independent of surrounding mural cells. These findings not only elucidate the mechanism underlying vascular dysfunction in Progeria but also provide insight into the molecular machinery that governs nuclear repositioning during sprouting angiogenesis.

Previous work targeting the LINC complex identified an abundance of Sun proteins in the membrane of Progeric nuclei. Several groups have attempted to disrupt Sun binding to Nesprins to rescue the forces acting on the nucleus.[5,21] In our hands, we observe an increase in Sun, but

we also observe a striking, and very reproducible, loss of perinuclear vimentin as well as a reduction in Nesprin coverage. The reduction in vimentin coverage was most evident during sprouting angiogenesis, potentially due to the dynamic cellular state and accelerated vimentin reassembly occurring during this process. Furthermore, in individual knockouts of LINC complex proteins this loss of interface significantly alters nuclear shape, and, in this cell type, it is not a viable option to ablate nuclear interfacing with the cytoskeleton.

The identification of vimentin dysfunction provides insight into the abnormal actin organization observed throughout the cell body. Vimentin intermediate filaments and actin exhibit a well-established interplay, in which vimentin interacts with contractile actomyosin arcs that drive the perinuclear localization of the vimentin network.[19,30] Consistent with this relationship, our data show that inhibition of either vimentin or actin alters the localization and phosphorylation status of the other. These findings suggest that coordinated regulation of both cytoskeletal systems is required to support efficient nuclear mobility.

Importantly, this observation provides our first mechanistic link to normal aging. A recent case study reported that a vimentin mutation (1160T>C) results in a premature aging phenotype, implicating vimentin dysfunction in age-related pathology.[9] In addition, our analysis of aged (24-month) mouse aortic endothelium revealed disrupted perinuclear vimentin organization. Together, these findings identify vimentin-mediated nucleo–cytoskeletal coupling as a potential contributor to vascular aging and highlight an important avenue for future investigation.

The mechanism underlying the accumulation of Sun proteins concurrent with reduced Nesprin coverage remains unclear. One possibility is that Progerin accumulation impairs Sun turnover, as Chen and colleagues report no change in mRNA levels in Progeric cells.[8] Alternatively, the accumulation of Sun may compromise its capacity to form functional trimers within the nuclear membrane, thereby reducing its capacity to engage Nesprins. It is also conceivable that increased nuclear membrane stiffness in Progerin expressing cells disrupts Nespin anchorage. Future studies are warranted to distinguish among these potential mechanisms.

The farnesyltransferase inhibitor, Lonafarnib, is not specific to Progerin and ultimately inhibits numerous cellular protein farnesylation. Farnesylation is particularly necessary during development, hence why the drug is not administered until after a year of development. However, our work shows that developmental processes are greatly impacted by Progerin, therefor a treatment which can be administered earlier is necessary. Progerinin is a newly developed drug which is specific to inhibition of Progerin, and not Lamin-A or other proteins and could be a viable option for earlier treatment. We first observed a positive effect when passaging cells and the cell number for patient cells treated with Progerinin was higher than untreated. Lonafarnib was detrimental so vessel sprouting, however Progerinin improved multiple parameters for patient sprouts. Progerinin treatment is far less harmful and seems to improve endothelial cell function.

The relevance of this work to aging biology merits consideration. Although Progeria is a distinct genetic disorder and does not fully recapitulate physiologic aging, it models several core biological mechanisms that occur more gradually during normal aging. These include genomic instability, low-level Progerin accumulation, progressive deterioration of nuclear morphology, as

well as shared defects in nuclear architecture observed in both patients with Progeria and elderly individuals.[25,27] Elucidation how nuclear structural defects, independent of other aging-associated issues, impact cellular function may clarify their contribution to organismal aging and highlight the nuclear envelope as a potential therapeutic target.

Methods

Reagents

All reagents, drugs, siRNA, and plasmid information are listed tables 1-4 of associated supplementary information.

Cell Culture

HEK cells were purchased from ATCC and cultured in Dulbecco's Modified Medium (DMEM) supplemented with 10% fetal bovine serum. Normal Human Lung Fibroblasts (NHLF's) were purchased from Lonza and cultured in Lonza FGM-2 Fibroblast Growth Medium-2 Bullet Kit®. Pooled Human umbilical vein endothelial cells (HUVECs) were purchased from PromoCell and cultured in proprietary media for 2–5 passages. Isolated mouse brain endothelial cells, as well as iPSC-derived endothelial cells, were cultured in PromoCell EGM-2 for 1-2 passages. All cells were maintained in a humidified incubator at 37 °C and 5% CO2. All medias contained 1% penicillin/ streptomycin and were used within 2-3 weeks of opening.

Small interfering RNA was resuspended to a 20 μM stock concentration and used at 0.5 μM. SiRNA was introduced into primary HUVEC's using electroporation with the Neon® transfection system (ThermoFisher). In vitro drug treatment concentrations are provided in Supplementary Table 3.

iPSC Differentiation

Patient iPSC's were acquired from the Progeria Research Foundation cell and tissue bank. We utilized cells belonging to the same donors (HGADFN167 iPS 1J, HGFDNFN168 iPS1 D2) for all experimental replicates. Differentiation of iPSC's was achieved following the protocol described in the Stem Cell Technologies STEMdiff™ Endothelial Differentiation Kit. Following differentiation, cells were split once prior to experimentation and not passaged more than two times in total. Experimental replicates for all iPSC-derived endothelium are the result of 3 separate differentiations from 3 vials received.

Mouse Endothelial Cell Isolation

Endothelial cell isolations were achieved by harvesting the brain of P6 mice. Mice were euthanized by decapitation, and the brain was quickly removed and stored in ice cold DMEM and transported to a sterile hood. The brain is mechanically reduced using a pestle, followed by progressively smaller syringes. Following mechanical reduction, homogenate was pelleted and resuspended with type II collagenase/dispase and digested for 1 hour with DNAse. The reaction was stopped with ice-cold DMEM and digestion was passed through a cell strainer.

Isolation of brain endothelium began with incubation with myelin removal beads, followed by CD45 coated beads (for removal of immune cells which are CD31 positive) and finally with

CD31 coated beads to isolate the endothelium. Upon isolation cells were incubated in EGM-2 media supplemented with puromycin (10ug/mL).

In Vitro & Ex Vivo Sprouting Angiogenesis Assay

Sprouting angiogenesis/ fibrinogen-bead assays were performed as reported by Nakatsu et al.[29] HUVECs were coated onto Cytodex-3 microcarrier beads (Cytvia) over 4 hours and plated overnight. SiRNA-treatment or viral transduction was performed the same day the beads were coated (Supplementary Table 1). Coated microbeads were embedded in a fibrinogen/aprotinin matrix in a 10cm live imaging dish. Once the clot was formed media was overlaid along with 100,000 NHLFs. Media was changed every other day along with monitoring of sprout development. Fixation occurred after 7 days post embedding. Ex Vivo and iPSC-derived sprouting assay protocols did not differ; however, both assays were extended from 7 days to 10 days.

Mosaic siRNA sprouting assays were achieved by treating a population of cells with Cell Tracker (ThermoFisher) and immediately electroporating siRNA into only cell tracker treated cells. These cells are then combined with untreated cells 50:50 and promptly coated onto beads the same day.

Sprout numbers were determined by counting the number of multicellular sprouts emanating from an individual microcarrier beads across multiple beads in each experiment. Sprout lengths were determined by measuring the length of a multicellular sprout beginning from the tip of the sprout to the microcarrier bead surface across multiple beads. Percent of non-lumenized sprouts were determined by quantifying the proportion of multicellular sprouts whose length (microcarrier bead surface to sprout tip) was less than 70% lumenized across multiple beads. Lumen diameters were determined by measuring the widest point in the vessel sprout, or at the location of a mosaic cell. Experimental repeats are defined as an independent experiment in which multiple cultures, containing numerous sprouting beads were quantified; this process of quantifying multiple parameters across many beads and several cultures was replicated on different days for each experimental repeat.

Lentivirus Generation & Transduction

Lentiviral plasmids were either purchased from Addgene or cloned by using the LR Gateway Cloning method. For lentiviral generation genes of interest and fluorescent proteins were isolated and incorporated into a pME backbone via Gibson reaction. Following confirmation of the plasmid by sequencing the pME entry plasmid was mixed with the destination vector and LR Clonase. The destination vector used in this study was pLEX 307. Once validated, the destination plasmids were transfected with the three required viral protein plasmids: pVSVG (gift from Bob Weinberg; Addgene plasmid #8454) and psPAX2 (gift from Didier Trono; Addgene plasmid #12260) into HEK 293 cells. The transfected HEKs had media changed 4 h post transfection. Transfected cells incubated for 3 days, and virus was harvested by virus concentration media and a 1-hour centrifugation in a fixed rotor at 4 Celsius.[18]

Cell Stimulation Assay

Treated HUVEC's were lysed at baseline, serum starvation, or 10 minutes stimulated. For baseline, cells were lysed without intervention, maintained in EGM-2 media. Serum-starvation, and stimulation, consisted of 2 hours incubation with OPTI-MEM. Following starvation cells were either lysed (starved condition) or received a media change with EGM-2 and allowed to incubate for 10 minutes (stimulated condition). Cells were lysed as described in immunoblotting protocol.

Mouse Husbandry

Mice for this investigation were housed in the Yale Animal Resources Center (YARC) under a 12-hour light/dark cycle at an ambient temperature of 20-24 °C. The mouse strain used throughout the study was C57BL/6-Tg(LMNA*G608G) and was purchased from Jackson Laboratories (Strain #: 010667). The donating investigator to the Jackson Laboratory was Dr. Francis Collins of the National Institute of Health. Offspring were genotyped by standard PCR from tail or ear DNA. All experimental procedures were reviewed and approved by IACUC.

Primer Name	**Sequence**	**Binding Site**
Common Forward	TTG GAC CAA ACA AGT ACA TAT CA	Mouse Chr4
Wildtype Reverse	CCA ATG ATA GTG ACA GGT ATA CGG	Mouse Chr4
Mutant Reverse	CTG ACA TTC TAG TGG AGG GAG A	Human LMNA

Developmental Angiogenesis & Vascular Profiling

Neonatal pups were euthanized by decapitation at P6 for developmental angiogenesis analysis of mouse retinas. P6 eyes were fixed with 4% paraformaldehyde (PFA) and constant agitation for 10 minutes, washed and promptly dissected for immunohistochemistry (IHC). Profiling of the adult vasculature was achieved by euthanizing 20-week, or 10-week, mice with isoflurane. Adult retinas were fixed with 4% PFA for 1 hour with constant agitation and retinas were dissected promptly following fixation.

Vascular perfusion assays for pup and adult mice were achieved by intraperitoneal injection of Sulfo-NHS-Biotin (5mg/g of body weight) resuspended in PBS. Following resuspension, Sulfo-NHS-Biotin was used the same day and not stored for later use. Incubation required 1-hour (pups) or 2-hours (adults) before euthanasia. Sulfo-NHS-Biotin was detected with IHC by Alexa Fluor-conjugated streptavidin.

Male and female mice were used for all experiments and no significant sex differences were evident in our quantification.

Live and Fixed Microscopy

All fluorescence microscopy was performed on an inverted Nikon Eclipse Ti2 microscope (Nikon Instruments) with a Perfect Focus System, equipped with a Dragonfly unit. Lasers were coupled into a multimode fiber going through the Andor Borealis unit reshaping the beam from a Gaussian profile to a homogenous flat top. As dichroic mirror, a CR-DFLY-DMQD-01 was used. Fluorescence light was spectrally filtered with an emission filter (TR-DFLY-F600-050) and imaged with a scientific complementary metal oxide semiconductor (sCMOS) camera (Sona 4BV6X, Andor Technologies). For live imaging, the microscope was equipped with a Okolab live

imaging chamber and an internal environment of 5% CO2 and 37 degrees Celsius was maintained.

Image processing was performed on FIJI (Image J) and IMARIS. Nuclei were segmented and 3D modeled using the IMARIS Surface Rendering feature. Live imaging analysis of nuclear movement was achieved by modeling nuclei with the surface rendering tool and running advanced statistics in IMARIS which provided sphericity, track straightness, track length, displacement and volume change data.

In Vitro & In Vivo Immunostaining

For immunofluorescence imaging, 2-dimensional HUVEC assays were fixed with 4% PFA for 7 min. ECs were then washed three times with PBS and permeabilized with 0.5% Triton-X (Sigma) for 10 min. After permeabilization, cells were washed three times with PBS. ECs were then blocked with 2% bovine serum albumin (BSA) for 30 min. Once blocked, primary antibodies were incubated for 2 hours, washed thrice and incubated with secondary antibodies for 1 hour. Washed and imaged. 3-dimensional sprouting assays were fixed for 40 minutes, washed three times and permeabilized for 1-2 hours (antibody dependent). Following permeabilization, sprouts were blocked for a minimum 1-hour before overnight primary antibody incubation. Thereafter, primary antibodies were removed, and the cells were washed 3 times with PBS. Secondary antibody with 2% BSA were added and incubated overnight, washed 3 times with PBS, and imaged. All primary and secondary antibodies are listed in Supplementary Table 3.

Following fixation, pup and adult retinas were washed and blocked with in vivo blocking buffer (1% Triton-X100, 5% BSA, and 5% donkey serum in PBS) for 1 hour. After blocking, retinas were incubated in primary antibody for 4 hours, or overnight, washed 3-5 times (antibody dependent) and treated with secondary for 4 hours. Retinas were then washed and mounted for imaging. Fluorescent imaging of proliferative cells was achieved with the Click-iT™ EdU Cell Proliferation Kit (Invitrogen) and provided protocol.

Adult aortas were isolated and trimmed of surrounding adipose. Aortas were fixed with 4% PFA for 20 minutes and blocked with in vivo blocking buffer for 30 minutes. Primary antibody incubated for 4 hours, aortas were washed 3 times, then secondary antibody treatment for 2-3 hours (antibody dependent) followed by washes and mounting.

In Vitro & In Vivo Immunoblotting

HUVEC's from stimulation assays and knockdown confirmations were lysed with cell scraper using RIPA buffer containing 1× PhosSTOP™ tablets (Sigma) and cOmplete™, Mini, EDTA-free Protease Inhibitor Cocktail tablets (Sigma). Cell lysate was vortexed and centrifuged for 10 minutes and supernatant was transferred to new tube.

Western blotting of HUVEC and iPSC-derived endothelial cell nuclear and cytosolic fractions were achieved by NE-PER™ Nuclear and Cytoplasmic Extraction Reagents kit.

Mouse retina lysate was acquired by removal and timely dissection of the retina in PBS. Retinas were gently transferred to a microcentrifuge tube and excess PBS removed. Both retinas from a

single mouse were combined and lysed with the previously described RIPA cocktail. Lysate was vortexed, centrifuged for 10 minutes, and supernatant transferred to a new vial.

For all specimens, lysate was brought up with Lamelli and incubated in a heat block at 98 degrees for 3-4 minutes. All samples were used within one week of preparation.

Statistical Analysis

In vitro experiments were repeated a minimum of three times. In vivo biological replicates were a minimum of 3, but mostly 5 or more. Statistical analysis and graphing were performed using GraphPad Prism. Statistical significance was assessed with a student's unpaired t-test for a two-group comparison. Multiple group comparisons were carried out using a one-way analysis of variance (ANOVA) followed by a Dunnett multiple comparisons test. Data was scrutinized for normality using Kolmogorov–Smirnov test. Statistical significance set a priori at $p < 0.05$.

Ethical Consideration

All research presented followed guidelines outlined by the Yale University Institutional Biosafety Committee (IBC) and Institutional Animal Care and Use Committee (IACUC).

References

1. Augustin, Hellmut G., and Gou Young Koh. "A systems view of the vascular endothelium in health and disease." Cell 187.18 (2024): 4833-4858.
2. Benedicto, Ignacio, Beatriz Dorado, and Vicente Andrés. "Molecular and cellular mechanisms driving cardiovascular disease in Hutchinson-Gilford progeria syndrome: lessons learned from animal models." Cells 10.5 (2021): 1157.
3. Booth-Gauthier, Elizabeth A., et al. "Hutchinson–Gilford progeria syndrome alters nuclear shape and reduces cell motility in three dimensional model substrates." *Integrative Biology* 5.3 (2013): 569-577.
4. Carley, Emma, et al. "The LINC complex transmits integrin-dependent tension to the nuclear lamina and represses epidermal differentiation." *elife* 10 (2021): e58541.
5. Chai, Ruth Jinfen, et al. "Disrupting the LINC complex by AAV mediated gene transduction prevents progression of Lamin induced cardiomyopathy." Nature Communications 12.1 (2021): 4722.
6. Chancellor, T. J., et al. "Actomyosin tension exerted on the nucleus through nesprin-1 connections influences endothelial cell adhesion, migration, and cyclic strain-induced reorientation." *Biophysical journal* 99.1 (2010): 115-123.
7. Chang, Wakam, et al. "Imbalanced nucleocytoskeletal connections create common polarity defects in progeria and physiological aging." *Proceedings of the National Academy of Sciences* 116.9 (2019): 3578-3583.
8. Chen, Chia-Yen, et al. "Accumulation of the inner nuclear envelope protein Sun1 is pathogenic in progeric and dystrophic laminopathies." *Cell* 149.3 (2012): 565-577.
9. Cogné, Benjamin, et al. "A dominant vimentin variant causes a rare syndrome with premature aging." European Journal of Human Genetics 28.9 (2020): 1218-1230.

10. Denis, Kevin B., et al. "The LINC complex is required for endothelial cell adhesion and adaptation to shear stress and cyclic stretch." *Molecular biology of the cell* 32.18 (2021): 1654-1663.
11. Dos Santos, Ália, and Christopher P. Toseland. "Regulation of nuclear mechanics and the impact on DNA damage." *International Journal of Molecular Sciences* 22.6 (2021): 3178.
12. Eriksson, Maria, et al. "Recurrent de novo point mutations in lamin A cause Hutchinson–Gilford progeria syndrome." *Nature* 423.6937 (2003): 293-298.
13. Fong, Loren G., et al. "Prelamin A and lamin A appear to be dispensable in the nuclear lamina." *The Journal of clinical investigation* 116.3 (2006): 743-752.
14. Gonzalo, Susana. "DNA damage and lamins." *Cancer biology and the nuclear envelope: recent advances may elucidate past paradoxes* (2014): 377-399.
15. Grunewald, Myriam, et al. "Counteracting age-related VEGF signaling insufficiency promotes healthy aging and extends life span." Science 373.6554 (2021): eabc8479.
16. Hamczyk, Magda R., Lara Del Campo, and Vicente Andrés. "Aging in the cardiovascular system: lessons from Hutchinson-Gilford progeria syndrome." Annual review of physiology 80 (2018): 27-48.
17. Hennekam, Raoul CM. “Hutchinson-Gilford progeria syndrome: review of the phenotype.” American journal of medical genetics Part A 140.23 (2006): 2603-2624
18. Jiang, Wei, et al. "An optimized method for high-titer lentivirus preparations without ultracentrifugation." Scientific reports 5.1 (2015): 13875.
19. Jiu, Yaming, et al. "Bidirectional interplay between vimentin intermediate filaments and contractile actin stress fibers." Cell reports 11.10 (2015): 1511-1518.
20. Kang, So-mi, et al. "Progerinin, an optimized progerin-lamin A binding inhibitor, ameliorates premature senescence phenotypes of Hutchinson-Gilford progeria syndrome." *Communications biology* 4.1 (2021): 5.
21. Kim, Paul H., et al. "Disrupting the LINC complex in smooth muscle cells reduces aortic disease in a mouse model of Hutchinson-Gilford progeria syndrome." Science translational medicine 10.460 (2018): eaat7163.
22. King, Samantha J., et al. "Nesprin-1 and nesprin-2 regulate endothelial cell shape and migration." *Cytoskeleton* 71.7 (2014): 423-434.
23. Kubben, Nard, et al. "Mapping of lamin A-and progerin-interacting genome regions." *Chromosoma* 121.5 (2012): 447-464.
24. Maier, Jeanette A., et al. "Aging and vascular disease: a multidisciplinary overview." Journal of Clinical Medicine 12.17 (2023): 5512.
25. Martins, Filipa, et al. "Nuclear envelope dysfunction and its contribution to the aging process." Aging cell 19.5 (2020): e13143.
26. Mironov, Alexander A., et al. "Intracellular membrane transport in vascular endothelial cells." *International journal of molecular sciences* 24.6 (2023): 5791.
27. Mosevitsky, M. I. "Progerin and its role in accelerated and natural aging." Molecular Biology 56.2 (2022): 125-146.
28. Musich, Phillip R., and Yue Zou. "Genomic instability and DNA damage responses in progeria arising from defective maturation of prelamin A." *Aging (Albany NY)* 1.1 (2009): 28.

29. Nakatsu, Martin N., et al. "Angiogenic sprouting and capillary lumen formation modeled by human umbilical vein endothelial cells (HUVEC) in fibrin gels: the role of fibroblasts and Angiopoietin-1☆." *Microvascular research* 66.2 (2003): 102-112.
30. Serres, Murielle P., et al. "F-actin interactome reveals vimentin as a key regulator of actin organization and cell mechanics in mitosis." Developmental cell 52.2 (2020): 210-222.
31. Shah, Pragya, et al. "Nuclear deformation causes DNA damage by increasing replication stress." *Current Biology* 31.4 (2021): 753-765.
32. Song, Minjung, et al. "Shear stress-induced mechanotransduction protein deregulation and vasculopathy in a mouse model of progeria." *Stem Cell Research & Therapy* 5.2 (2014): 41.